BioMedical Engineering OnLine

RESEARCH

Open Access

Long-term inhaling ultrafine zinc particles increases cardiac wall stresses elevated by myocardial infarction

Songyu Wang[1,2†], Haifang Wang[1†], Li Li[2,3], Pei Niu[2,3], Zhongjie Yin[4] and Yunlong Huo[2,3*]

†Songyu Wang and Haifang Wang share the first authorship.

*Correspondence: huoyunlong@sjtu.edu.cn

[1] School of Control Engineering, Northeastern University at Qinhuangdao, Qinhuangdao, China
[2] Institute of Mechanobiology & Medical Engineering, School of Life Sciences & Biotechnology, Shanghai Jiao Tong University, Shanghai, China
[3] PKU-HKUST Shenzhen-Hong Kong Institution, Shenzhen, Guangdong, China
[4] Department of Chemical Engineering, Imperial College London, London, UK

Abstract

The analysis of cardiac wall mechanics is of importance for understanding coronary heart diseases (CHD). The inhalation of ultrafine particles could deteriorate CHD. The aim of the study is to investigate the effects of cardiac wall mechanics on rats of myocardial infarction (MI) after long-term inhalation of ultrafine Zn particles. Cardiac wall stresses and strains were computed, based on echocardiographic and hemodynamic measurements. It was found that MI resulted in the significantly elevated stresses and the reduced strains. The short-term inhalation of ultrafine Zn particles decreased stresses and increased strains in MI rats, but the long-term inhalation had the opposite effects. Hence, the short-term inhalation of ultrafine Zn particles could alleviate the MI-induced LV dysfunction while the long-term inhalation impaired it.

Introduction

Coronary heart disease (CHD) of high morbidity and mortality increased in China because of aging [1, 2]. Exposure to ultrafine particles (PM0.1) in air pollution was known to have possibility of deteriorating CHD [3–5]. We have recently shown significant left ventricle (LV) dysfunctions in rats of myocardial infarction (MI), based on the speckle tracking echocardiography (STE) and histological measurements [6–8]. Since the environmental monitoring found a high concentration of trace metal element, Zn, in air pollution in Shanghai [9], the STE analysis in cardiac strains showed possibility of the retarded progression of LV dysfunctions in MI rats by the short-term inhalation of ultrafine Zn particles, but the impairment of LV dysfunctions by the long-term inhalation [6]. In comparison with the strain analysis, cardiac wall stress can quantify LV functions better [10–12]. There is, however, lack of a study to analyze the corresponding changes of LV wall mechanics completely.

The distribution of cardiac wall stress is of importance for understanding the changes of CHD [13, 14]. Taking advantage of the merit of computational wall mechanics has been used to quantify ventricular biomechanical properties in cardiovascular diseases [15–18]. The LV wall mechanics characterized the elevated diastolic LV stiffness and the

slowed LV relaxation in rats of heart failure [19, 20]. A vicious cycle of increased cardiac wall stress and LV dysfunctions could prompt the development of heart failure [8, 11, 19].

The objective of the study is to investigate the changes of cardiac wall stress in rats of MI after long-term inhalation of ultrafine Zn particles. We hypothesized that short-term inhalation of ultrafine Zn particles alleviated the increased cardiac wall stress caused by the MI, but the long-term inhalation significantly increased the stress accelerating the LV dysfunctions. To test the hypothesis, we demonstrated the analysis of LV wall mechanics (including Cauchy stress and Green strain) using the Continuity software (UCSD CMRG Group, San Diego, USA), based on echocardiographic and hemodynamic measurements. The significance and limitation of the study were discussed relevant to effects of inhaling ultrafine zinc particles on myocardial wall mechanics in rats of MI.

Results

Table 1 lists a significant increase of LVEDP caused by myocardial infarction despite of no statistical difference in the four Sham groups. The LVEDP in the MI4 group is higher than the MIZn4 group (15.9 ± 1.12 vs 10.8 ± 1.50 mmHg) while the value in the MI6 group is lower than the MIZn6 group (19.8 ± 2.03 vs 25.9 ± 1.17 mmHg). Figure 1 shows the ED pressure–volume relationships between computational results and estimations based on the Klotz's method in representative animals of the eight groups, showing strong correlations in Table 2. Passive material parameters show no statistical difference between the four Sham groups in Table 1. Material constant, C_{pas}, is significantly higher in the four MI groups than the sham groups. Material constant, C_{pas}, increases in a sequence of MIZn4, MI4, MI6, and MIZn6.

Figure 2 shows representative distribution of ED Cauchy stress in the eight groups. Figure 3a–c shows ED Cauchy stresses in the entire LV, MI zone, and non-infarction zone, respectively. Table 3 lists ED Cauchy stresses along the longitudinal direction from the base to apex regions and along the radial direction from the endocardium to epicardium. Cardiac Cauchy stresses are significantly higher in the four MI groups than the four Sham groups, which increase with time. The MI zone has higher stresses than the non-MI zone. The MIZn6 group has the highest cardiac stresses than other groups.

Table 1 Passive material constants and LVEDP

Groups	C_{pas} (kPa)	b_f	b_t	b_{fs}	LVEDP (mmHg)
Sham4	0.06 ± 0.04	74 ± 8	3.3 ± 1.2	16 ± 8	2.0 ± 0.5
ShamZn4	0.07 ± 0.02	80	3.0	31 ± 18	2.6 ± 0.9
MI4	0.50 ± 0.35*	16 ± 12*	9 ± 5*	32 ± 15*	16 ± 1*
MIZn4	0.46 ± 0.22◆	16 ± 6◆	13 ± 5◆	37 ± 17	11 ± 2◆#
Sham6	0.06 ± 0.04	72 ± 10	4.3 ± 1.6	26 ± 6	3.0 ± 0.5
ShamZn6	0.06 ± 0.03	75 ± 6	4.3 ± 1.6	27 ± 12	3.4 ± 0.4
MI6	0.53 ± 0.35*	34 ± 21*	7 ± 5	15	20 ± 2*
MIZn6	0.6 ± 0.35◆	12 ± 8◆#	9 ± 3◆	15 ± 8	26 ± 1◆#

All of the data are shown as mean ± SD

* P < 0.05, MI vs Sham

# P < 0.05, MIZn vs MI

◆P < 0.05, ShamZn vs MIZn

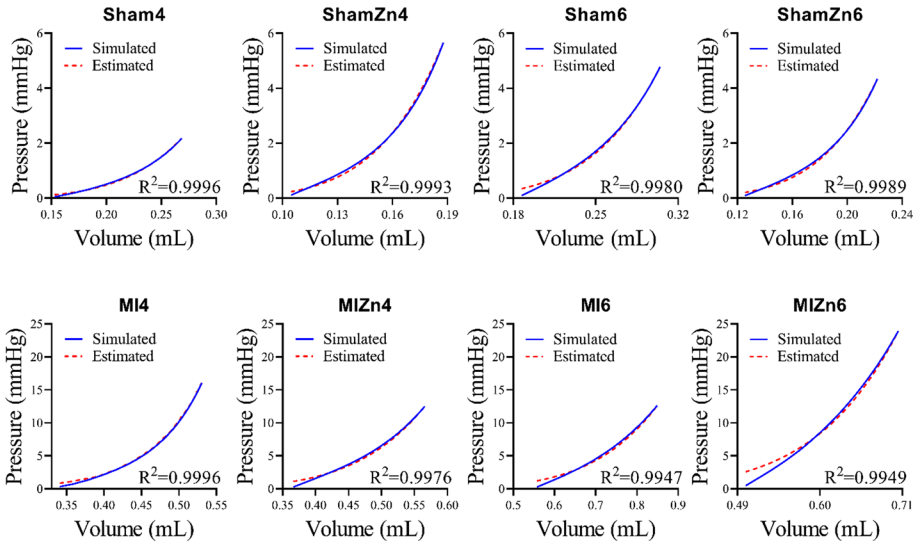

Fig. 1 A comparison of computed and Klotz ED pressure–volume curves in representative animals of the eight groups

Table 2 Difference between computed and Klotz ED pressure–volume relationships

Groups	R^2	RMS/LVEDP (%)	Groups	R^2	RMS/LVEDP (%)
Sham4	0.9992 ± 0.0003	6.3 ± 1.6	Sham6	0.9983 ± 0.0005	6.9 ± 1.1
ShamZn4	0.9993 ± 0.0003	7.2 ± 2.2	ShamZn6	0.9981 ± 0.0011	6.5 ± 1.4
MI4	0.9978 ± 0.0041	6.9 ± 1.5	MI6	0.9969 ± 0.0022	6.9 ± 1.9
MIZn4	0.9991 ± 0.0008	7.5 ± 1.2	MIZn6	0.9975 ± 0.0017	7.5 ± 1.9

All the data are shown as mean ± SD

RMS Root mean square

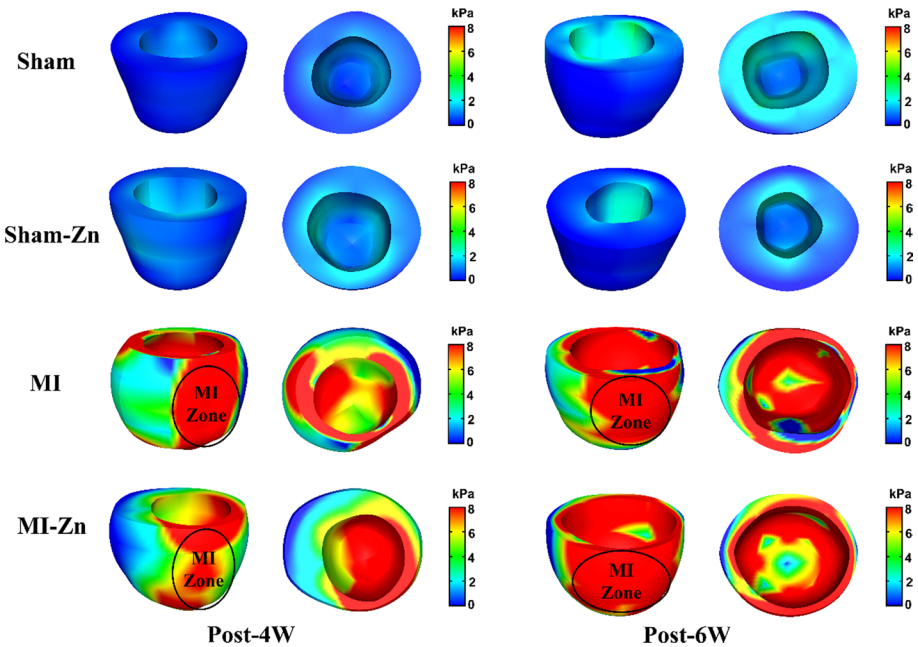

Fig. 2 The distribution of ED Cauchy stress in representative animals of the eight groups

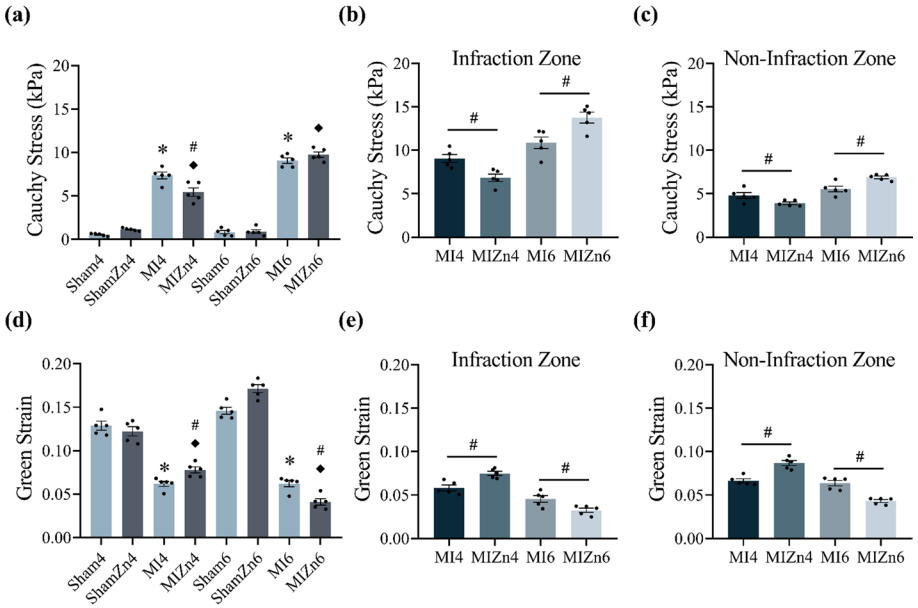

Fig. 3 **a**–**c** The ED Cauchy stress in the entire LV (**a**), MI zone (**b**), and normal zone (**c**); **d**–**f** the ED Green strain in the entire LV (**d**), MI zone (**e**), and normal zone (**f**). All the data are shown as mean ± SEM. *P < 0.05, MI vs Sham; ◆P < 0.05, ShamZn vs MIZn; #P < 0.05, MIZn vs MI

Table 3 Cauchy stresses and Green strains along the longitudinal direction from the base to apex regions and along the radial direction from the endocardium to epicardium

Groups	Base	Middle	Apex	Endocardium	Middle wall	Epicardium
Cauchy stresses						
Sham4	0.8 ± 0.2	0.9 ± 0.2	0.44 ± 0.10	1.7 ± 0.4	0.8 ± 0.2	0.51 ± 0.06
ShamZn4	0.9 ± 0.2	1.1 ± 0.2	0.53 ± 0.10	1.7 ± 0.3	0.66 ± 0.11	0.51 ± 0.08
MI4	7.2 ± 0.1*	6.6 ± 0.3*	6.1 ± 0.2*	8.6 ± 0.3*	5.8 ± 0.1*	4.9 ± 0.1*
MIZn4	6.3 ± 0.2◆^	5.7 ± 0.2◆^	5.3 ± 0.1◆^	7.5 ± 0.3◆^	4.6 ± 0.1◆^	4.0 ± 0.1◆^
Sham6	1.0 ± 0.4	1.2 ± 0.7	0.56 ± 0.37	1.4 ± 0.7	0.50 ± 0.25	0.43 ± 0.25
ShamZn6	0.7 ± 0.4	0.9 ± 0.5	0.49 ± 0.27	1.4 ± 0.7	0.54 ± 0.37	0.47 ± 0.33
MI6	8.1 ± 0.7*#	8.1 ± 0.9*#	7.9 ± 0.8*#	10 ± 2*#	8.3 ± 0.9#	8.2 ± 0.7*
MIZn6	12 ± 1◆^	11 ± 2◆	9.4 ± 1.6◆	15 ± 2◆^	11 ± 1◆^	9.2 ± 0.7◆^
Green strains						
Sham4	0.12 ± 0.01	0.11 ± 0.01	0.1 ± 0.01	0.24 ± 0.04	0.1 ± 0.02	0.09 ± 0.01
ShamZn4	0.1 ± 0.01	0.11 ± 0.01	0.1 ± 0.02	0.25 ± 0.04	0.09 ± 0.01	0.08 ± 0.006
MI4	0.06 ± 0.003*	0.07 ± 0.01*	0.05 ± 0.003*	0.09 ± 0.002*#	0.06 ± 0.001*	0.06 ± 0.003*
MIZn4	0.07 ± 0.002◆	0.08 ± 0.01◆	0.06 ± 0.002◆	0.12 ± 0.01◆	0.07 ± 0.008◆	0.07 ± 0.005
Sham6	0.1	0.1	0.09 ± 0.003	0.24	0.1	0.08 ± 0.003
ShamZn6	0.1	0.09 ± 0.002	0.09 ± 0.002	0.25 ± 0.01	0.09 ± 0.008	0.08 ± 0.005
MI6	0.05 ± 0.004*	0.06 ± 0.006*	0.04 ± 0.005*	0.08 ± 0.002*#	0.06 ± 0.001*#	0.05 ± 0.002*#
MIZn6	0.04 ± 0.01◆	0.04 ± 0.01◆^	0.02 ± 0.007◆^	0.06 ± 0.005◆^	0.03 ± 0.007◆^	0.03 ± 0.006◆^

All the data are shown as mean ± SD

* P < 0.05, MI vs Sham

# P < 0.05, MI vs MIZn

◆P < 0.05, MIZn vs ShamZn

^P < 0.05, MIZn6 vs MIZn4

Cardiac stresses in the MIZn4 group are lower than the MI4 group. The endocardium has significantly higher stresses than the middle and epicardium.

Figure 3d–f shows ED Green strains in the entire LV, MI zone, and non-infarction zone, respectively. Table 3 lists Green strains along the longitudinal direction from the base to apex regions and along the radial direction from the endocardium to epicardium. Green strains are significantly lower in the four MI groups than the four Sham groups. The MI zone has lower strains than the non-MI zone. The endocardium has higher strains than the middle and epicardium. The MIZn6 group has lower strains than the MI6 group, while the MIZn4 group has higher values than the MI4 group. Green strains in the MIZn6 group are remarkably lower than the MIZn4 group.

Discussion

Myocardial contraction and relaxation regulated the heart's pumping functions [13, 21]. Here, the effect of inhaling ultrafine zinc particles on cardiac wall stresses and strains at diastole was evaluated in MI rats using the computational mechanics model. The major findings were reported as: (1) MI significantly increased cardiac Cauchy stresses; (2) long-term inhalation of ultrafine zinc particles accelerated the MI-induced increase of stresses; and (3) short-term inhalation alleviated the MI-induced increase of stresses.

Cardiac ED Cauchy stresses in the four MI groups were higher than the Sham groups and the stresses in the MI region as well as the border zone were significantly higher than normal zones, consistent with the findings of previous studies [8, 22, 23]. Myofibroblasts were mainly localized in MI and border zones [24]. Fibroblast migration to the border zone was mediated by growth factors and proinflammatory cytokines, which were associated with the increased stresses [25]. An increase of stresses in MI and border zones could also activate interstitial fibroblasts, promoting a matrix-synthetic phenotype and contributing to scar maturation in the MI zone and myocardial fibrosis in the border zone. The changes of Cauchy stresses were caused by two major risk factors, i.e., the increased LVEDP and the MI-induced wall stiffening in MI and border zones. The long-term inhaling zinc particle caused excessive Zn accumulation in heart tissue, which stimulated the transformation of fibroblasts into myofibroblasts and accelerated production and remodeling of extracellular matrix [26, 27], resulting in myocardial fibrosis [28–31]. We have experimentally shown a significant increase of myocardial fibrosis in MI rats owing to the long-term inhalation of ultrafine Zn particles [6]. This study showed an increase of the corresponding fiber stresses in both MI and non-infarction regions as well as along the radial direction from the endocardium to epicardium. The long-term elevation of ED fiber stress could lead to fiber elongation, chamber enlargement, and hypertrophy [32] and destroy the supply–demand balance in the entire myocardium [33]. Hence, the long-term inhalation of ultrafine Zn particles deteriorated the cardiac mechanics functions in MI rats. In contrast, since the MI-activated atrial natriuretic peptide led to a decrease of Zn concentrations in serum and heart tissue [34], the short-term inhalation of ultrafine Zn particles could replenish Zn concentrations and hence slow down the development of LV dysfunctions and remodeling in both MI and non-infarction regions [6, 7]. Accordingly, this study showed the reduction of cardiac stresses in both MI and non-infarction regions by the short-term inhalation of ultrafine Zn particles, which alleviated LV dysfunctions.

The STE analysis found the MI-induced decrease of global myocardial strains in our previous studies [6, 7]. Accordingly, this study showed the decrease of local ED Green strains, which characterized the weakened myocardial deformation owing to the MI-induced wall stiffening. The increased fiber stress led to abnormal biological responses to stimulate myocardial fibrosis [35–37] and enlarged the scarring region and deteriorated LV dysfunctions [8, 11]. The decreased strain could compensate for the significant increase of stress in order to protect from the MI impairments partially. The strain varied in inverse proportion to the changes of stress in MI rats after the inhalation of ultrafine Zn particles.

Critiques of the study: The STE analysis of cardiac strains and strain rates showed the changes of both systolic and diastolic functions in MI rats after the inhalation of ultrafine Zn particles [6]. This study only computed ED Cauchy stresses and Green strains and did not consider the systolic values in the LV of the eight groups. The study also neglected the computation in the RV. The following studies should demonstrate the computational wall mechanics over a cardiac cycle in the entire heart as well as carry out more experimental measurements to find the relevant mechanobiology mechanisms to the changes of cardiac stress and strain.

Conclusions

The analysis of computational wall mechanics demonstrated an increase of Cauchy stresses by 1044% and a decrease of Green strains by 58% in MI rats as compared with the shams on average. In MI rats, the short-term inhalation of ultrafine Zn particles showed a 23% reduction in stresses and a 30% increase in strains and the long-term inhalation had the opposite effects, resulting in a 20% increase in stresses and a 29% decrease in strains. This study supported the findings that the short-term inhalation of ultrafine Zn particles alleviated the MI-induced LV dysfunction while the long-term inhalation deteriorated it. This shed light on understanding the effect of air pollution on heart health and could provide new strategies for inhibiting the development of myocardial infarction, potentially enhancing patient's life quality.

Methods

Experimental measurements

Figure 4a shows schematic representation of experimental measurements. Wistar male rats (6 weeks, Beijing Vital River Laboratory) were used in the study, animal preparation, and echocardiographic and hemodynamic experimental protocols were similar to our previous study [6]. Briefly, myocardial infarction was created through ligation of the left anterior descending (LAD) artery under anesthesia. Shams underwent similar operation without the LAD ligation. There were four groups: sham group (Sham), sham with inhalation of ultrafine Zn particles (ShamZn), myocardial infarction group (MI), and MI with inhalation of ultrafine Zn particles (MIZn). We designed an equipment comprised of the container, ultrasonic nebulizer and electric air pump to control the inhalation of ultrafine Zn particles, as shown in Fig. 4a. The equipment exposed the ShamZn and MIZn groups in the environment filled with ultrafine zinc particles at a concentration of 500 $\mu g/m^3$ from 10:00 AM to 2:00 PM, randomly selecting 4 days per week.

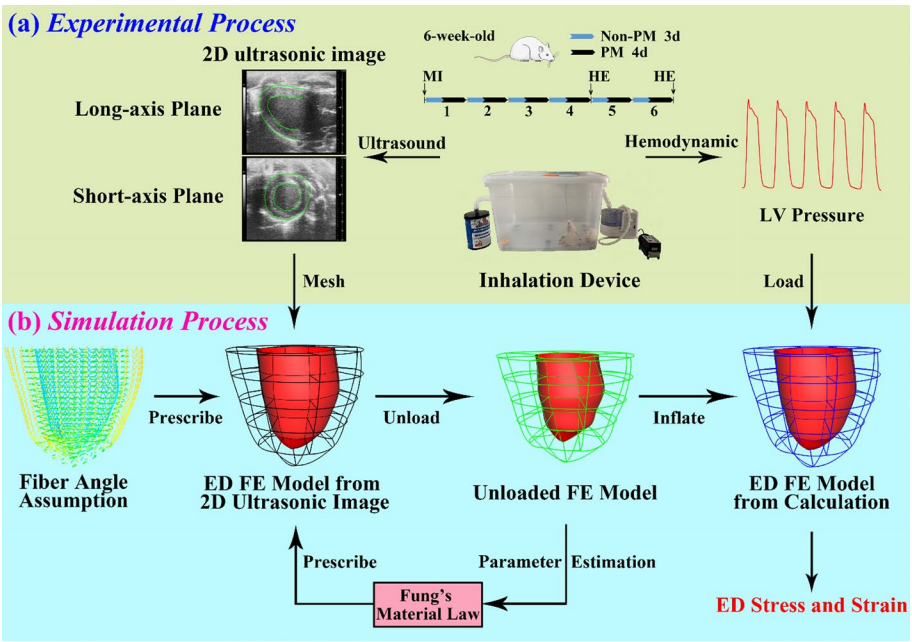

Fig. 4 Schematic representation of experimental measurements and cardiac wall mechanics computation. **a** Animal preparation and echocardiographic and hemodynamic measurements; **b** the flow chart of cardiac wall mechanics computation

We carried out a preliminary echocardiographic measurement in the MIZn group for 2, 4 and 6 weeks after the LAD ligation. Animals inhaling ultrafine Zn particles for ≤ 4 weeks had the opposite effects to those for 6 weeks. Hence, the four groups were further divided into two subgroups, i.e., postoperative 4 weeks and 6 weeks (animals were terminated for 4 or 6 weeks after MI surgery). The eight groups ($n = 5$ in each group) were: Sham4, ShamZn4, MI4, MIZn4, Sham6, ShamZn6, MI6 and MIZn6. Here, long-term exposure was established from 4 weeks onwards, i.e., Sham6, ShamZn6, MI6 and MIZn6 groups.

Based on M-mode tracings, we determined the end-diastolic (ED) endocardial and epicardial contours. The scarring zone in MI rats was defined based on the wall thickness, i.e., the average ED normal ventricular wall thickness subtracted by $2.5 \times$ SD (2.5 times standard deviation) [38]. The non-infarction zone is the area except for the scarring zone. The LV ED pressure (LVEDP) was recorded by a Millar catheter.

All experiments were performed in accordance with The Chinese National and Shanghai Jiao Tong University ethical guidelines regarding the use of animals in research, in agreement with the NIH guidelines (Guide for the care and use of laboratory animals) on the protection of animals used for scientific purposes. The experimental protocol was approved by the Animal Care and Use Committee of Shanghai Jiao Tong University, China.

Cardiac wall biomechanics computation

Figure 4b shows the flow chart of cardiac wall mechanics computation. First, the 3D geometrical model of LV wall is generated from the ED endocardial and epicardial contours and meshed with cubic-Hermite finite elements, where the fiber direction is modeled by

the coordinate frame interpolation [19]. The geometrical model of unload LV wall is estimated from the ED model [39]. The strain energy function is written as follows:

$$\mathrm{W} = \frac{C_{pas}}{2}\left(\mathrm{e}^{\mathrm{Q}} - 1\right) + \frac{k}{2}(J\mathrm{In}J - \mathrm{In}J) \tag{1}$$

$$\mathrm{Q} = b_f E_{ff}^2 + b_t\left(E_{cc}^2 + E_{tt}^2 + E_{ct}^2 + E_{tc}^2\right) + b_{fs}(E_{fc}^2 + E_{cf}^2 + E_{ft}^2 + E_{tf}^2) \tag{2}$$

Parameters C_{pas}, b_f, b_t and b_{fs} are absolute constants independent of deformation and position, where C_{pas} represents the stiffness of the myocardial material, b_f affects the stiffness in the transverse direction of the fibers, b_t influences the stiffness in the radial direction of the fibers, and b_{fs} impacts the stiffness when subjected to shear stress. The normal zone has material constant of C_{pas} and the scarring zone has material constant of $10 \cdot C_{pas}$ [40]. Linear interpolation is used to transition the material constant smoothly between the normal and scarring zones across the border zone [11]. Parameters $E_{ij}^2(i.j = f, c, t)$, k (=350 kPa), and J represent Green strains along the fiber, cross-fiber and transverse-fiber directions, bulk modulus, and Jacobian of deformation gradient tensor, respectively. Second, material parameters, C_{pas}, b_f, b_t and b_{fs}, are determined in all animals of the eight groups by the pattern search method [41], where the difference between the computed ED pressure–volume relationship and the one defined by Klotz [15] is set to the objective function, as shown in Fig. 1. Finally, LVEDP is incrementally applied to the endocardium to compute the changes of LV stress and strain in all animals of the eight groups.

Statistical analysis

Experimental measurements were repeated three times in each animal. All parameters were presented as mean ± SEM by averaging over all animals in each group. A two-way ANOVA (Sigma Stat 3.5) was used to demonstrate the statistical difference of morphometric and hemodynamic parameters between the eight groups, where P value < 0.05 was indicative of a significant difference.

Author contributions

S.W. and Z.Y. carried out computation and prepared figures, L.L. and P.N. performed experimental measurements, and H.W. and Y.H. wrote and reviewed the manuscript. All the authors reviewed the manuscript.

Funding

This work is supported by the National Key Research and Development Program of China 2021YFA1000200 and 2021YFA1000203 (Y. Huo) and Shenzhen Science and Technology R&D Grant KQTD20180411143400981 (Y. Huo).

Availability of data and materials

All data are available from the corresponding author upon request.

Declarations

Ethics approval and consent to participate

All the experiments were performed in accordance with Chinese National and Shanghai Jiao Tong University ethical guidelines regarding the use of animals in research, in agreement with the NIH guidelines (Guide for the care and use of laboratory animals) on the protection of animals used for scientific purposes. The experimental protocol was approved by the Animal Care and Use Committee of Shanghai Jiao Tong University, China.

Competing interests

The authors declare no competing interests.

Received: 18 September 2023 Accepted: 29 July 2024
Published online: 05 August 2024

References

1. Mendis S, Davis S, Norrving B. Organizational update: the world health organization global status report on non-communicable diseases 2014; one more landmark step in the combat against stroke and vascular disease. Stroke. 2015;46(5):e121–2.
2. Moran A, Zhao D, Gu D, Coxson P, Chen CS, Cheng J, Liu J, He J, Goldman L. The future impact of population growth and aging on coronary heart disease in China: projections from the coronary heart disease policy model-China. BMC Public Health. 2008;8:394.
3. Andre N. Toxic potential of materials at the nanolevel. Science. 2006;311(5761):622–7.
4. Karottki DG, Bekö G, Clausen G, Madsen AM, Andersen ZJ, Massling A, Ketzel M, Ellermann T, Lund R, Sigsgaard T, et al. Cardiovascular and lung function in relation to outdoor and indoor exposure to fine and ultrafine particulate matter in middle-aged subjects. Environ Int. 2014;73:372–81.
5. Franck U, Odeh S, Wiedensohler A, Wehner B, Herbarth O. The effect of particle size on cardiovascular disorders—the smaller the worse. Sci Total Environ. 2011;409(20):4217–21.
6. Huo Y, Li L. Long-term inhalation of ultrafine zinc particles deteriorated cardiac and cardiovascular functions in rats of myocardial infarction. Front Physiol. 2022;13: 921764.
7. Li L, Niu P, Wang X, Bing F, Tan W, Huo Y. Short-term inhalation of ultrafine zinc particles could alleviate cardiac dysfunctions in rats of myocardial infarction. Front Bioeng Biotechnol. 2021;9: 646533.
8. Wang X, Li L, Zhao Y, Tan W, Huo Y. The interplay of cardiac dysfunctions and hemodynamic impairments during the progression of myocardial infarction in male rats. J Biomech. 2022;142: 111237.
9. Ming LL, Jin L, Li J, Fu PQ, Yang WY, Liu D, Zhang G, Wang ZF, Li XD. PM2.5 in the Yangtze river delta, China: chemical compositions, seasonal variations, and regional pollution events. Environ Pollut. 2017;223:200–12.
10. Packer M, O'Connor C, McMurray JJV, Wittes J, Abraham WT, Anker SD, Dickstein K, Filippatos G, Holcomb R, Krum H, et al. Effect of ularitide on cardiovascular mortality in acute heart failure. N Engl J Med. 2017;376(20):1956–64.
11. Zhao DL, Niu P, Sun XT, Yin ZJ, Tan WC, Huo YL. Mechanical difference of left ventricle between rabbits of myocardial infarction and hypertrophy. J Biomech. 2020;111: 110021.
12. Van Vuren EJ, Malan L, Von Kanel R, Cockeran M, Malan N. Hyperpulsatile pressure, systemic inflammation and cardiac stress are associated with cardiac wall remodelling in an African male cohort: the SABPA study. J Hypertens. 2016;34: e115.
13. Sack KL, Davies NH, Guccione JM, Franz T. Personalised computational cardiology: patient-specific modelling in cardiac mechanics and biomaterial injection therapies for myocardial infarction. Heart Fail Rev. 2016;21(6):815–26.
14. Alter P, Rupp H, Rominger MB, Czerny F, Vollrath A, Klose KJ, Maisch B. A new method to assess ventricular wall stress in patients with heart failure and its relation to heart rate variability. Int J Cardiol. 2010;139(3):301–3.
15. Klotz S. Single-beat estimation of end-diastolic pressure-volume relationship: a novel method with potential for noninvasive application. Circulation. 2006;94(1):2497–506.
16. Krishnamurthy A, Villongco C, Beck A, Omens J, Mcculloch A. Left ventricular diastolic and systolic material property estimation from image data: LV mechanics challenge. In: Camara O, Mansi T, Pop M, Rhode K, Sermesant M, Young A, editors. Statistical atlases and computational models of the heart: imaging and modelling challenges : 5th international workshop STACOM 2014, held in conjunction with MICCAI 2014, Boston, MA, USA, september 18, 2014, revised selected papers. Cham: Springer International Publishing; 2015.
17. Lee LC, Genet M, Dang AB, Ge L, Guccione JM, Ratcliffe MB. Applications of computational modeling in cardiac surgery. J Card Surg. 2014;29(3):293–302.
18. Kassab GS, Algranati D, Lanir Y. Myocardial-vessel interaction: role of LV pressure and myocardial contractility. Med Biol Eng Comput. 2013;51(7):729–39.
19. Yin Z, Zhang W, Zhao D, Sulejmani F, Feng Y, Huo Y, Tan W. Cardiac wall mechanics analysis in hypertension-induced heart failure rats with preserved ejection fraction. J Biomech. 2020;98: 109428.
20. Bing F, Wang X, Shen W, Li L, Niu P, Chen Y, Zhang W, Tan W, Huo Y. Inhalation of ultrafine zinc particles impaired cardiovascular functions in hypertension-induced heart failure rats with preserved ejection fraction. Front Bioeng Biotechnol. 2020;8:13.
21. Lee LC, Kassab GS, Guccione JM. Mathematical modeling of cardiac growth and remodeling. Wiley Interdiscip Rev Syst Biol Med. 2016;8(3):211–26.
22. Wang ZNJ, Wang VY, Bradley CP, Nash MP, Young AA, Cao JJ. Left ventricular diastolic myocardial stiffness and end-diastolic myofibre stress in human heart failure using personalised biomechanical analysis. J Cardiovasc Transl Res. 2018;11(4):346–56.
23. Wenk JF, Sun K, Zhang ZH, Soleimani M, Ge LA, Saloner D, Wallace AW, Ratcliffe MB, Guccione JM. Regional left ventricular myocardial contractility and stress in a finite element model of posterobasal myocardial infarction. J Biomech Engin Trans Asme. 2011;133(4): 044501.
24. Blankesteijn WM, EssersJanssen YPG, Verluyten MJA, Daemen MJAP, Smits JFM. A homologue of drosophila tissue polarity gene frizzled is expressed in migrating myofibroblasts in the infarcted rat heart. Nat Med. 1997;3(5):541–4.
25. Humeres C, Frangogiannis NG. Fibroblasts in the infarcted, remodeling, and failing heart. JACC Basic Transl Sci. 2019;4(3):449–67.
26. Rao BG. Recent developments in the design of specific matrix metalloproteinase inhibitors aided by structural and computational studies. Curr Pharm Des. 2005;11(3):295–322.
27. Yang F, Xue YJ, Wang FL, Guo DN, He YJ, Zhao X, Yan FY, Xu YQ, Xia DD, Liu YS. Sustained release of magnesium and zinc ions synergistically accelerates wound healing. Bioact Mater. 2023;26:88–101.

28. Burrough ER, De Mille C, Gabler NK. Zinc overload in weaned pigs: tissue accumulation, pathology, and growth impacts. J Vet Diagn Invest. 2019;31(4):537–45.
29. Hasegawa H, Suzuki K, Suzuki K, Nakaji S, Sugawara K. Effects of zinc on the reactive oxygen species generating capacity of human neutrophils and on the serum opsonic activity in vitro. Luminescence. 2000;15(5):321–7.
30. Lindsey ML. MMP induction and inhibition in myocardial infarction. Heart Fail Rev. 2004;9(1):7–19.
31. Brieger A, Rink L, Haase H. Differential regulation of TLR-dependent MyD88 and TRIF signaling pathways by free zinc ions. J Immunol. 2013;191(4):1808–17.
32. Grossman W. Cardiac hypertrophy: useful adaptation or pathologic process? Am J Med. 1980;69(4):576–84.
33. Jan KM. Distribution of myocardial stress and its influence on coronary blood flow. J Biomech. 1985;18(11):815–20.
34. Ripa S, Ripa R, Giustiniani S. Are failured cardiomyopathies a zinc-deficit related disease? a study on Zn and Cu in patients with chronic failured dilated and hypertrophic cardiomyopathies. Minerva Med. 1998;89(11–12):397–403.
35. Han Y, Huang K, Yao QP, Jiang ZL. Mechanobiology in vascular remodeling. Natl Sci Rev. 2018;5(6):933–46.
36. Venugopal H, Hanna A, Humeres C, Frangogiannis NG. Properties and functions of fibroblasts and myofibroblasts in myocardial infarction. Cells. 2022;11(9):1386.
37. Schumacher D, Kramann R. Multiomic spatial mapping of myocardial infarction and implications for personalized therapy. Arterioscler Thromb Vasc Biol. 2023;43(2):192–202.
38. Baer FM, Smolarz K, Theissen P, Voth E, Schicha H, Sechtem U. Regional Tc-99m-methoxyisobutyl-isonitrile-uptake at rest in patients with myocardial infarcts—comparison with morphological and functional parameters obtained from gradient-echo magnetic-resonance-imaging. Eur Heart J. 1994;15(1):97–107.
39. Krishnamurthy A, Gonzales MJ, Sturgeon G, Segars WP, McCulloch AD. Biomechanics simulations using cubic Hermite meshes with extraordinary nodes for isogeometric cardiac modeling. Comput Aided Geometric Des. 2016;43:27–38.
40. Genet M, Chuan Lee L, Ge L, Acevedo-Bolton G, Jeung N, Martin A, Cambronero N, Boyle A, Yeghiazarians Y, Kozerke S. A novel method for quantifying smooth regional variations in myocardial contractility within an infarcted human left ventricle based on delay-enhanced magnetic resonance imaging. J Biomech Eng. 2015;137(8): 081009.
41. Audet C, Dennis JE. Analysis of generalized pattern searches. SIAM J Optim. 2002;13(3):889–903.

Publisher's Note